JACS
JOURNAL OF THE AMERICAN CHEMICAL SOCIETY
Article
pubs.acs.org/JACS

Residue-Dependent Adsorption of Model Oligopeptides on Gold

Kenan P. Fears,[†] Thomas D. Clark,*[,†] and Dmitri Y. Petrovykh*[,†,‡]

[†]Division of Chemistry, Naval Research Laboratory, Washington, D.C. 20375, United States
[‡]Department of Physics, University of Maryland, College Park, Maryland 20742, United States

Supporting Information

ABSTRACT: The adsorption to gold surfaces in aqueous solutions has been systematically evaluated for a series of model oligopeptides. The series includes GG−X−GG "host-guest" sequences, where the central X residue is one of 19 proteinogenic amino acids, and water-soluble X_5 and X_{10} homo-oligopeptides. Irreversible adsorption on gold of GG−X−GG peptides, which lack significant secondary structure, was quantitatively analyzed by X-ray photoelectron spectroscopy (XPS). The broad range of the quasi-equilibrium surface densities measured by XPS corroborates the hypothesis that surface interactions of GG−X−GG peptides are dominated by their central X residues. The highest surface density was produced by GGCGG, followed by sequences with hydrophobic, charged, and polar central residues. Neither electrostatic nor hydrophobic interactions dominate the adsorption of GG−X−GG peptides: for charged and polar central residues, surface densities correlate with the size of the side chains but not with the sign of the charges, while for hydrophobic residues, the surface densities are uncorrelated with side-chain hydrophobicity. An intriguing result is the disparity in surface adsorption of structural isomers of Leu and Val, which exhibit a correlation between the position of the branched carbon in the side chain and the interaction of the peptide backbone with the surface. The surface density produced by the adsorption of GG−X−GG peptides overall was low; however, adsorption tended to increase as the number of X residues increased (GG−X−GG < X_5 < X_{10}), suggesting that cooperative binding is important for surface attachment of proteins that readily adsorb on inorganic surfaces. The Leu and Val isomer investigation and trends revealed by our analysis show how the methodology and results described here provide a fundamental reference for future experimental and computational studies and for rational design of peptides that exhibit predictable adsorption behaviors on a given surface.

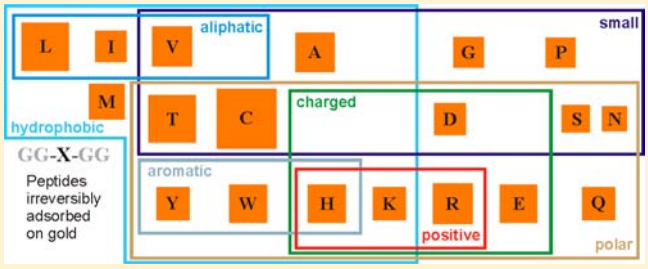

INTRODUCTION

The aim of this work is to discover how the proteinogenic amino acid residues differ in their propensity to adsorb to inorganic surfaces. Over the past few decades, some generalizations have emerged concerning selective interactions between specific amino acid side chains and surfaces. Addadi and Weiner noted in a seminal paper that proteins containing acidic residues are closely associated with calcium-containing biomineral formation *in vivo*,[1] an observation that led to many *in vitro* investigations of mineralization using biomimetic agents such as carboxylic-acid-containing peptides.[2−4] The preferential interaction of carboxylic-acid residues with inorganic oxide surfaces appears to be a general phenomenon, as several groups have used phage display technology in recent years to select short, acidic peptides that bind preferentially to oxides such as titania and silica.[5] Other phage display studies have determined that aromatic residues are important for selective interaction with the surfaces of carbon-based materials such as graphene and carbon nanotubes.[6−9]

The specific examples notwithstanding, few systematic studies have been carried out with the aim of identifying contributions of individual residues to adsorption behavior of peptides. Results from investigations of single amino acids and short sequences (di- and tripeptides) are limited by their relevance to longer peptides in which residues experience a more "protein-like" environment.[10−12] Willett and co-workers[13] examined the differential adhesion to inorganic surfaces of homo-oligopeptides eight to ten residues in length, using fluorophores attached to the N-termini to quantify surface adsorption. However, these authors did not discuss possible contributions to adhesion from nascent secondary structure,[14−18] free C-termini, or the presence of the large, polycyclic fluorophores at the N-termini of their peptides. Additionally, using fluorophores to quantify adsorption is problematic when the surfaces examined are metals such as gold, which are known to quench fluorescence.[19,20]

Here, we aim to further understand residue-specific peptide−surface interactions by systematically and quantitatively analyzing the interactions of carefully chosen model peptides with a model surface. To minimize the potential effects of secondary structure and to isolate the effect of an individual amino acid residue on peptide adsorption, we selected the well-known GG−X−GG "host-guest"[21−24] peptide system that NMR spectroscopists have long used as a model of unstructured peptide conformations.[25−27] The flanking G

Received: May 1, 2013
Published: September 30, 2013

   dx.doi.org/10.1021/ja404346p | J. Am. Chem. Soc. 2013, 135, 15040−15052

(glycine) residues provide a peptide environment for the central guest residue, X, yet induce minimal secondary structure,[21,22,26,27] allowing us to systematically assess the effect of the central guest residue on peptide adsorption. We also avoided contributions to adsorption from free N- and C-termini by protecting these functionalities via acetylation and amidation, respectively.[28] Of the 20 possible proteinogenic guest residues, 19 of the GG−X−GG peptides (having capped N- and C-termini, as mentioned above) are water-soluble, the exception being GG−F−GG. Accordingly, we used these 19 sequences as our principle set of model peptides; where possible, we supplemented the GG−X−GG model set with those homo-oligopeptides (penta- and decamers, denoted hereafter as X_5 and X_{10}, respectively) that proved to be water-soluble.

We chose polycrystalline gold as our model surface because it can be readily cleaned and it is not adversely affected by an extended immersion in aqueous buffers. Gold surfaces are also technologically important, for example, in biosensors based on surface plasmon resonance (SPR) or quartz crystal microbalance (QCM). Organic films adsorbed on gold surfaces may be interrogated using standard analytical techniques of surface science, including X-ray photoelectron spectroscopy (XPS)—the primary technique used here. In prior work, we extensively validated the use of XPS for quantifying the adsorption of oligonucleotides to gold surfaces;[29−34] these experiences strongly suggested that we could fruitfully apply the combination of gold surfaces and XPS to study peptide adsorption as well.

We note that, in principle, we could have chosen techniques other than XPS for analyzing peptide adsorption to gold surfaces. Radiolabeled peptides, however, pose concerns over safety and generation of hazardous waste, while fluorescent labels suffer from the limitations mentioned above—that their fluorescence is quenched by gold surfaces and their large, polycyclic structures can potentially influence or even dominate the adsorption behavior of small peptides. Methods such as ellipsometry, SPR spectroscopy, and various QCM measurements are frequently used to determine the amount of adsorbates on a surface.[35−38] Unfortunately, these methods cannot quantify specifically the amount of peptide adsorbed on the surface. For example, adventitious hydrocarbons that readily adsorb to surfaces upon exposure to air can affect these measurements. When working with large adsorbates, such as proteins, hydrocarbon contaminants are typically considered negligible because proteins can often displace or mask the hydrocarbons; both of these putative effects arise from the much larger molecular weights of proteins compared to those of the hydrocarbons. However, the effect of adventitious hydrocarbon contaminants on the adsorption of *small* peptides has not been previously examined in detail. While *in situ* depositions can be used with the aforementioned techniques to eliminate exposure to air, cleaning the surfaces prior to peptide exposure can merely replace the hydrocarbons with detergent molecules that may or may not be displaced by adsorbing peptides, and SPR or QCM cannot conclusively identify the molecules present on the surface. In addition, SPR spectroscopy does not directly measure the mass of adsorbed material, but rather the change in refractive index at the surface. This change is, in turn, influenced by the surface polarity and charge density[39]—both of which are subject to change upon the adsorption of biomolecules.

Having selected suitable model peptides and a surface for our investigation of peptide adsorption, we developed sample preparation protocols that produce reliable and reproducible samples for quantitative measurements.[40] In the absence of secondary structure, we assumed that the surface adsorption of our model peptides is primarily directed by their intrinsic affinities for gold. The irreversible adsorption of model peptides on gold was then quantitatively analyzed by XPS, which provided elemental and chemically-specific data for evaluating the relative surface densities of surface-adsorbed peptides and for comparing the results across the entire set of model peptides and control samples. The results of our systematic survey of residue-dependent adsorption of model peptides on gold are presented in a series of charts, along with a master plot, followed by discussion and interpretation of the observed trends relating to side-chain chemistries.

EXPERIMENTAL SECTION

Materials. The peptides with N- and C-termini acetylated ($-COCH_3$) and amidated ($-NH_2$), respectively, were synthesized and purified (>98%) by GenScript USA Inc. All buffer reagents were used as received from Sigma-Aldrich Co. Stock solutions of the peptides were prepared using a 10 mM sodium phosphate buffer, adjusted to a pH of 7.0 by mixing the appropriate amounts of NaH_2PO_4 and Na_2HPO_4 solutions. We determined the peptide concentration in solution from the dry weight of lyophilized peptide added to buffer, following the methodology described elsewhere.[40]

Gold Substrates. We used gold-coated silicon (Au thickness of ca. 100 nm) wafers from Platypus Technologies as substrates for surface adsorption experiments. After cutting the wafers into pieces of ca. 1.0 cm^2, we cleaned the pieces by sequentially sonicating them for 5 min in each of the following solutions: 0.005% (v/v) Triton X-100, "piranha" wash [7:3 H_2SO_4 (98 wt %)/H_2O_2 (30 wt %)], and "RCA standard clean 1" [1:1:5 NH_4OH (28.0−30.0% NH_3 basis)/H_2O_2 (30 wt %)/H_2O]. (*Caution: piranha solution is extremely oxidizing, reacts violently with organics, and should only be stored in loosely covered containers to avoid pressure buildup.*) The substrates were thoroughly rinsed with 18 MΩ-cm deionized (DI) water after each sonication step and dried under a stream of nitrogen at the completion of the cleaning process. We cleaned all substrates immediately before the adsorption experiments to limit their exposure to contaminants in the atmosphere.

Preparation of Samples. We placed clean substrates into pure buffer solution in glass vials and added the appropriate amount of peptide stock solution to produce an incubation solution of roughly constant mass concentration: 1.0 mM for pentapeptides (GG−X−GG and X_5) and 0.5 mM for decapeptides (X_{10}). In preliminary adsorption experiments for a group of model peptides, we did not observe any significant difference in the surface density between 18 and 24 h incubations; thus, we selected incubation periods of 24 h as a point by which the surface-adsorbed peptides reach the maximum quasi-equilibrium surface density: the maximum density achievable under specified conditions that represents a steady-state (i.e., an apparent quasi-equilibrium) of partitioning between solution and surface concentrations of peptides. After the incubation period, we filled the vials to overflowing with DI water before withdrawing the substrates, effectively infinitely diluting the peptide solution to avoid passing the substrates through the air−water interface, where peptide molecules may have collected during the incubation period. We rinsed the substrates again with DI water after removing them from the incubation vials and dried the substrates under a stream of nitrogen.

Statistical Analysis. To derive statistical estimates of the reported values from measurements at multiple ($n \geq 3$) discrete points, all calculated values are reported as a mean plus or minus 95% confidence interval (C.I.) for $n \geq 3$. The same 95% level of statistical significance is used to identify differences between measured values in Student's unpaired *t*-tests ($p \leq 0.05$).

X-ray Photoelectron Spectroscopy. We acquired XPS data at room temperature in an ultra-high vacuum analysis chamber with the base pressure <5 × 10^{-9} mbar. A commercial XPS instrument was equipped with a monochromated Al Kα X-ray source, the energy of which was regularly calibrated and maintained at 1486.6 ± 0.2 eV. The microfocused X-ray source illuminated a spot of ca. 400 × 600 μm^2 on the substrate; we analyzed at least three separate positions for each sample. Survey spectra were acquired with 1 eV step size at a pass energy (PE) of 200 eV (ca. 1.7 eV resolution); we acquired high-resolution spectra with 0.15 eV step size at PE = 20 eV (ca. 0.5 eV resolution). The binding energy (BE) scale of this spectrometer was regularly calibrated based on an automated procedure to produce the Au $4f_{7/2}$, Cu $2p_{3/2}$, and Ag $3d_{5/2}$ peaks within <0.05 eV from the standard reference BE values.[41] The aliphatic C 1s peak was observed at BE = 284.4 ± 0.3 eV for peptide samples. We acquired normal-emission high-resolution spectra in the Au 4f, C 1s, N 1s, O 1s, and S 2p regions to determine the elemental and chemical composition of the peptide films.

In control experiments, we analyzed thick peptide films that were prepared by pipetting 3 μL drops onto warmed (ca. 75 °C) gold substrates. We analyzed these reference films as-prepared and after *in situ* sputtering for 15 s with low-energy Ar^+ ions (200 eV) to remove surface contaminants and reveal the bulk composition of the thick peptide films. Spatially uniform charge neutralization across these samples was provided by beams of low-energy (≤10 eV) electrons and Ar^+ ions; the charge neutralization device produced ca. 2 × 10^{-7} mbar partial pressure of Ar in the analysis chamber during measurements.

XPS Analysis and Quantification. We performed peak fitting of high-resolution spectra in Unifit (v 2011), using a convolution of Lorentzian and Gaussian line shapes to fit the individual components.[42] To produce consistent fits of minor C 1s components, which are superimposed on the inelastic background of the main peak, a linear combination of Shirley and linear functions with consistent parameters was used to model the background, which was included in the iterative fitting process. Multiple-component fitting in the C 1s region always started from the lowest-BE component and its full-width at half-maximum (fwhm) was used to constrain the fwhm's for the other components. The standard "atomic %" elemental compositions were quantified using calibrated analyzer transmission functions, Scofield sensitivity factors,[43] and effective attenuation lengths (EALs) for photoelectrons; EALs were calculated using the standard TPP-2M formalism.[44,45] Additional normalization for comparison of the XPS data across the model sets was performed based on the thin-overlayer approximation, i.e., assuming that the effect of XPS signal attenuation in the peptide overlayers is small and similar for all the samples. We note that the major contribution of signal attenuation that is relevant for comparison of intensities between different elements is accounted for by the EAL term in the atomic % calculation.[29] Accordingly, we used C/N and O/N ratios of atomic % values to evaluate the stoichiometry of each peptide film with respect to theoretical ratios based on full chemical formula of the peptide; N was chosen as the reference element specific to peptides and not subject to heavy contamination in our samples.[40] The global average value of Au atomic % for all peptide samples was 50 ± 1%, so the gold signal provided a nearly constant internal reference for all samples. The N/Au atomic % ratios were used to evaluate and compare the surface densities of the different model peptides; to compare the densities in terms of residues per surface area, the N/Au ratios were normalized by the average number of nitrogen atoms per residue in the respective peptides. Notably, the normalized N/Au signals indicate the coverage of less than one molecular layer for most of the peptides in this work, justifying our use of the thin-overlayer approximation. For adsorbed peptide films that exhibited the highest surface densities, neglecting the attenuation of the Au signal by the overlayer could result in overestimation of the surface density by ca. 10−15%.[31]

Circular Dichroism. We used CD spectroscopy to assess the secondary structure of the peptides in solution. UV absorbance and CD spectra were simultaneously collected using a Jasco J-815 spectrometer (JASCO, Inc.) over the wavelength range of 185−290 nm in a 1.0-mm path length quartz cuvette. Scans were acquired at a rate of 20 nm/min; each CD spectrum represents an accumulation of 5 scans. The temperature of the cuvette was maintained at 20 °C throughout analysis to minimize solvent evaporation and temperature fluctuations. We baseline-corrected all CD and absorbance spectra of the peptide solutions by subtracting the corresponding blank buffer spectrum. Baseline-corrected CD spectra were converted from raw ellipticity (Θ, mdeg) to molar ellipticity ([Θ], deg × cm^2/dmol) using the following equation:

$$[\Theta] = (\Theta \times \mathrm{MW})/(n_r \times 10000 \times C_{soln} \times L) \quad (1)$$

where MW is the molecular weight of the peptide (g/mol), C_{soln} is the peptide concentration (g/mL), L is the optical path length through buffer (cm), and n_r is the number of amino acid residues.

RESULTS AND DISCUSSION

Evaluation of Secondary Structure. Our goal of evaluating the intrinsic affinities of the specific peptide side chains for gold surfaces required minimizing the influence of peptide secondary structures on our adsorption experiments. We chose GG−X−GG sequences as the main model pentapeptides based on their previously reported lack of significant secondary structure in aqueous solutions;[27] for thoroughness, however, we performed solution CD measurements to confirm these earlier findings for our entire GG−X−GG series (Figure 1). We detected no bands in the spectrum of GGGGG and found that bands in the GG−X−GG spectra (Figure 1, left) were generally weak (we note that for X = G, X_5 and GG−X−GG sequences are equivalent). A noticeable exception is GGYGG, which exhibits positive bands near 205 and 230 nm that are due to contributions from the aromatic side-chain rather than the conformation of the peptide backbone;[46−48] a positive band around 225 nm is also observed for GGWGG. CD spectra showing strong negative bands near 195 nm and weak positive bands near 215 nm have been previously shown to correlate with polyproline II (PPII) structure.[26] These PPII bands were much more pronounced for X_5 homopentapeptides and X_{10} homodecapeptides (Figure 1, right) than for the corresponding GG−X−GG pentamers (Figure 1, left).

For G, R, D, K, and E peptides in the right panel of Figure 1, comparison of the homopentamer and homodecamer CD spectra (X_5 and X_{10} spectra are shown with solid and dashed lines, respectively) indicates a weak dependence, if any, of secondary structure on the chain length. Given that we normalized the CD spectra to mean molar ellipticity per residue, such small quantitative differences in otherwise qualitatively similar spectra for those X_5−X_{10} pairs suggest that no new secondary structures emerge for the longer decamers. The only exception to this weak dependence is decaserine, the CD spectrum of which exhibits features characteristic of an antiparallel β sheet, with a maximum at 195 nm and a single minimum at 221 nm. These extrema are close to the values of 197 and 222 nm, respectively, reported by Quadrifoglio and Urry for poly(L-serine) in water,[49] which is known to form antiparallel β sheets.[50]

Analysis of XPS Data. We chose XPS as the main method for quantitative analysis of surface-adsorbed peptides based on three main considerations. XPS and related electron spectroscopies have been previously used to obtain characteristic spectra from a variety of peptide samples on different substrates.[10,16,18,51−53] XPS also has been established and corroborated for quantitative analysis of DNA films,[29−34,54] which share with peptide films some of the challenging properties in terms of both preparation and analysis. Finally,

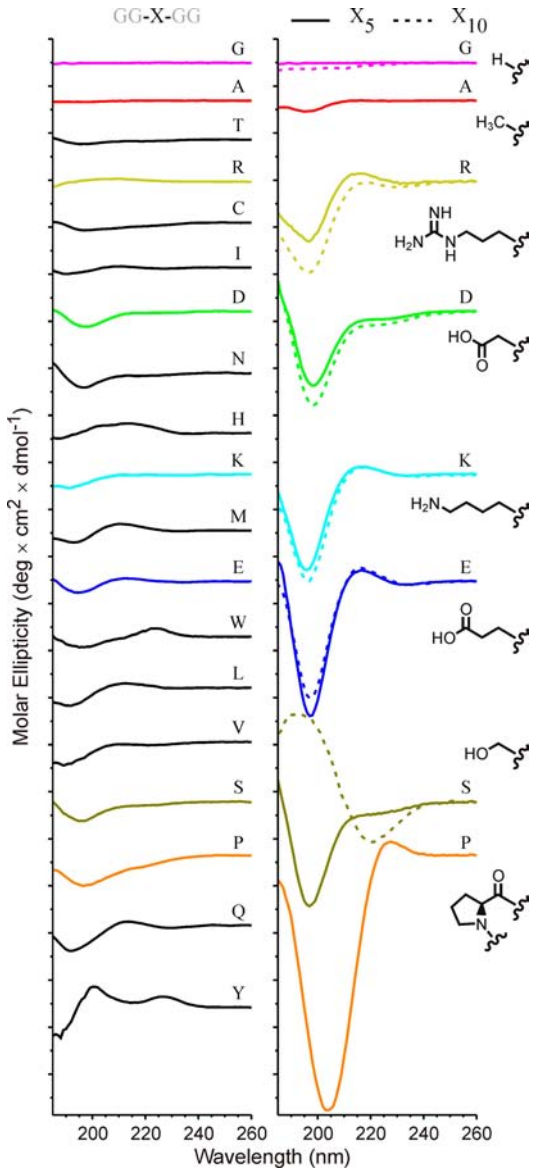

Figure 1. CD spectra of model oligopeptides in aqueous solutions. Water-soluble GG−X−GG (left panel), and X_5 (solid, right panel) and X_{10} (dashed, right panel) peptides (0.2 mM solutions in 10 mM sodium phosphate, pH = 7.0) were measured in a 1-mm path quartz cuvette at 20 °C. The spectra are color-coded and labeled based on the "X" residues (insets, right panel) in GG−X−GG, X_5, or X_{10} sequences. All spectra are normalized to show mean molar ellipticity per residue. Vertical offset is added to clarify the visual presentation; the molar ellipticity of each spectrum at 260 nm is approximately zero; each tick represents 5000 molar ellipticity units.

detailed evaluation of the elemental and chemical information in the XPS data allowed us to validate our protocols and methodology to systematically and reproducibly carry out the peptide adsorption experiments in this study.[40]

Figure 2 shows high-resolution XPS data for the Au 4f, C 1s, N 1s, O 1s, and S 2p regions for GGCGG adsorbed on gold surfaces from an aqueous buffer and for a blank-buffer control. As discussed in more detail later, GGCGG peptide produces the highest surface density and, accordingly, the strongest peptide-specific spectral features. The strong and sharp N1 component at BE = 399.8 eV (fwhm ≈ 1.5 eV) in the N 1s region is the clearest indication of the GGCGG peptide presence, as XPS peaks from nitrogen in amides and amines are expected to have BEs in this range.[10,16,31,51,52] In contrast, no peaks are observed in the N 1s region for the control sample that was incubated in a blank buffer. A similar comparison to the blank-buffer control also indicates that the C2−C4 components in the C 1s spectrum of GGCGG are predominantly peptide-specific, in agreement with the corresponding general ranges for carbon chemistries[10,16,52,55] expected in peptide samples: C−N and C−O groups contribute to C2 at BE = 286.0 eV, C═O groups to C3 at BE = 287.9 eV, and O—C═O groups together with other permutations of several C−N and C−O bonds contribute to C4 at BE = 289.4 eV. An additional Cys-specific C 1s component (C5) at 285.5 eV corresponds to C−S. The O 1s spectrum of the GGCGG sample differs dramatically from that of the blank-buffer control; the nontrivial amount of O observed for the latter, however, is notable and likely associated with contamination and physisorbed water.[40]

The S 2p region for the blank-buffer control in Figure 2 confirms that our deposition solutions and environment did not contribute any significant S-based contamination. Conversely, the S atom from the putative surface-attachment Cys residue (inset in Figure 2) clearly forms a thiolate bond with the gold surface, as indicated by a single sharp S 2p doublet at BE = 161.8 eV.[54,56,57] The absence of higher-BE S 2p components also confirms the absence of disulfides or free thiols[56] and hence of GGCGG peptides that are forming multilayers or are otherwise not attached to gold primarily via the thiolate bond of the Cys residue. Quantification of the S 2p signal for GGCGG is discussed in more detail in one of the subsequent sections.

Representative spectra from N 1s and C 1s regions, i.e., regions that contain the main peptide-specific XPS information, are shown in Figure 3 for all GG−X−GG, X_5, and X_{10} peptides in our study. The main peptide-specific N 1s component (N1) at 399.4−399.9 eV BE dominates the spectra for the majority of the sequences. A small component shifted to lower BE at 397.7−398.3 eV (N2, shaded in orange) is observed in many spectra and is consistent with amide/amine groups that are interacting with the gold surface via contacts that involve significant charge transfer.[29,31,40] Small components at 400.9−401.3 eV BE (N3, shaded in purple) observed for K and R peptides correspond to protonated amines.[40] In the C 1s region, the peptide-specific C2−C4 components are observed for all the sequences; however, in contrast with the GGCGG data in Figure 2, the aliphatic C1 component is the strongest C 1s component for all the other sequences, indicating that a significant amount of contamination is present in all samples.[40]

Accounting for Sample Contamination. Because the apparent surface affinities of our model peptides are relatively weak, contaminants could potentially interfere with our experiments by blocking adsorption. We conducted a series of control experiments to determine the source of surface contaminants so that we could establish protocols to minimize contamination of our surfaces, as described in detail elsewhere.[40] In particular, we found that the main sources of sample contamination in our experiments were adventitious adsorbates, which lead to an increasing amount of carbon and oxygen detected on gold with increasing exposure time to the ambient atmosphere. Carbonaceous adsorbates were detected on gold substrates that were exposed to ambient air for as little as 1 s after sputter-cleaning in ultra-high vacuum,[40] indicating that some level of surface contamination is unavoidable for

dx.doi.org/10.1021/ja404346p | J. Am. Chem. Soc. 2013, 135, 15040−15052

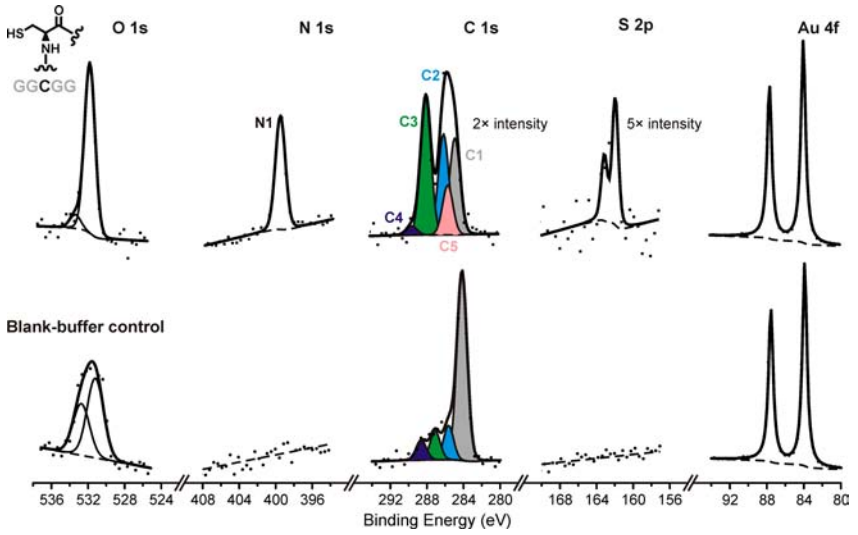

Figure 2. XPS data for GGCGG deposited on gold and a blank-buffer control. Elemental spectra and fits are shown to scale, unless otherwise noted, for the O 1s, N 1s, C 1s, and S 2p regions; Au 4f spectra are normalized with respect to the maximum intensity of the aqueous control. Symbols = data points, thick lines = overall fits, thin and shaded outlines = chemical components, dashed lines = backgrounds.

samples prepared in solutions under practical laboratory conditions. Accordingly, we decided to follow an alternative strategy of (1) verifying that the presence of (or competition against) contaminants did not significantly affect our peptide adsorption experiments, and (2) developing methods for validating and analyzing peptide-specific data obtained in the presence of surface contamination.[40]

Elemental ratios expected from theoretical stoichiometry (i.e., full chemical formulas corresponding to the model peptide sequences, including terminal acetylation and amidation) are shown in Figure 4 for each set of model peptides as hatched columns flanking the experimental data summarizing more detailed analyses of high-resolution spectra, such as those in Figures 2 and 3. In all cases, both C and O are over-represented in the adsorbed peptide (tabulated C/N and O/N ratios for all peptides are presented in the Supporting Information, Table S1), but the data show no simple or consistent correlation of the degree of contamination with physical or chemical properties of the peptides (e.g., peptide length, hydrophobicity or charge of side chains). The excess of oxygen, for example, would correspond to multiple water molecules per peptide residue, if water were assumed to be the main O-containing coadsorbate responsible for the O/N ratios in Figure 4. Such extreme excess of associated water is unlikely, particularly for sequences with hydrophobic side chains; thus, other coadsorbates are probably contributing to the oxygen signal. In general, the apparent sequence independence of the excess C and O signals suggests that similar levels of adventitious C and O contaminants may be observed for other samples of short peptides that are deposited and handled in laboratory-ambient environments.

The most prominent component in the C 1s spectra in Figure 3 is C1 with BE = 284.4 ± 0.3 eV, which corresponds to aliphatic (C−C) carbon.[31,40,55,56] An inspection of the side chain structures for the central "X" residues indicates that the GG−X−GG peptides themselves do not contain enough aliphatic carbon to dominate the C 1s spectra. To ensure that commercial peptide samples obtained at the highest available purity (>98%) did not contain significant levels of bulk or surface-active contaminants, we analyzed a set of representative control samples prepared as thick films of dried stock peptide solutions (as described in Experimental Section and in ref 40). These "dried drop" control samples were transferred into the XPS system within 15 min after preparation and thus show C/N and O/N ratios that are close to the "theoretical" ratios expected from stoichiometry (Figure 5). Removing the topmost ca. 0.5 nm of material from these dried drops by low-energy Ar^+ sputtering,[40,55] reveals the bulk composition of each peptide film (labeled as "sputtered drop" in Figure 5), which is also close to the "theoretical" ratio for all the peptides. In these and similar experiments for other sequences, we found no evidence of bulk or surface-active contaminants in high-purity peptide samples.

Examination of the XPS data in Figure 5 (bars labeled as "adsorbed") and Figure 3 indicates that samples with higher surface densities of peptides (GGCGG, GGLGG, and GGTGG) show lower amounts of excess C and O, which leads us to infer that adventitious contaminants are responsible for the excess C and O detected on the other samples. The apparent resistance to adventitious contamination is a common property of organic and biological monolayers with high surface densities.[29,31,56] Accordingly, we sought to correct ("corrected ads." in Figure 5) the observed elemental ratios for contributions of adventitious contamination, by subtracting from the data for "adsorbed" samples the levels of C- and O-containing signals that were measured on a blank-buffer control that was incubated in buffer for 24 h in the absence of any peptide (Figure 2, bottom). Albeit crude, this correction proved effective in bringing the experimental data into close agreement with theoretical elemental ratios ("corrected" versus "theoretical" bars in Figure 5) and accounted for the majority of the excess of C and O signals observed on GGKGG and GGEGG samples; the remaining discrepancies between the corrected and theoretical elemental ratios for these samples indicate that adsorbed films of some peptides may have low resistance to adventitious contamination.

Systematic Survey of Peptide Adsorption on Gold. The GG−X−GG model peptides allowed us to perform a broad survey of surface adsorption from aqueous buffer because they are water-soluble for 19 out of 20 proteinogenic amino

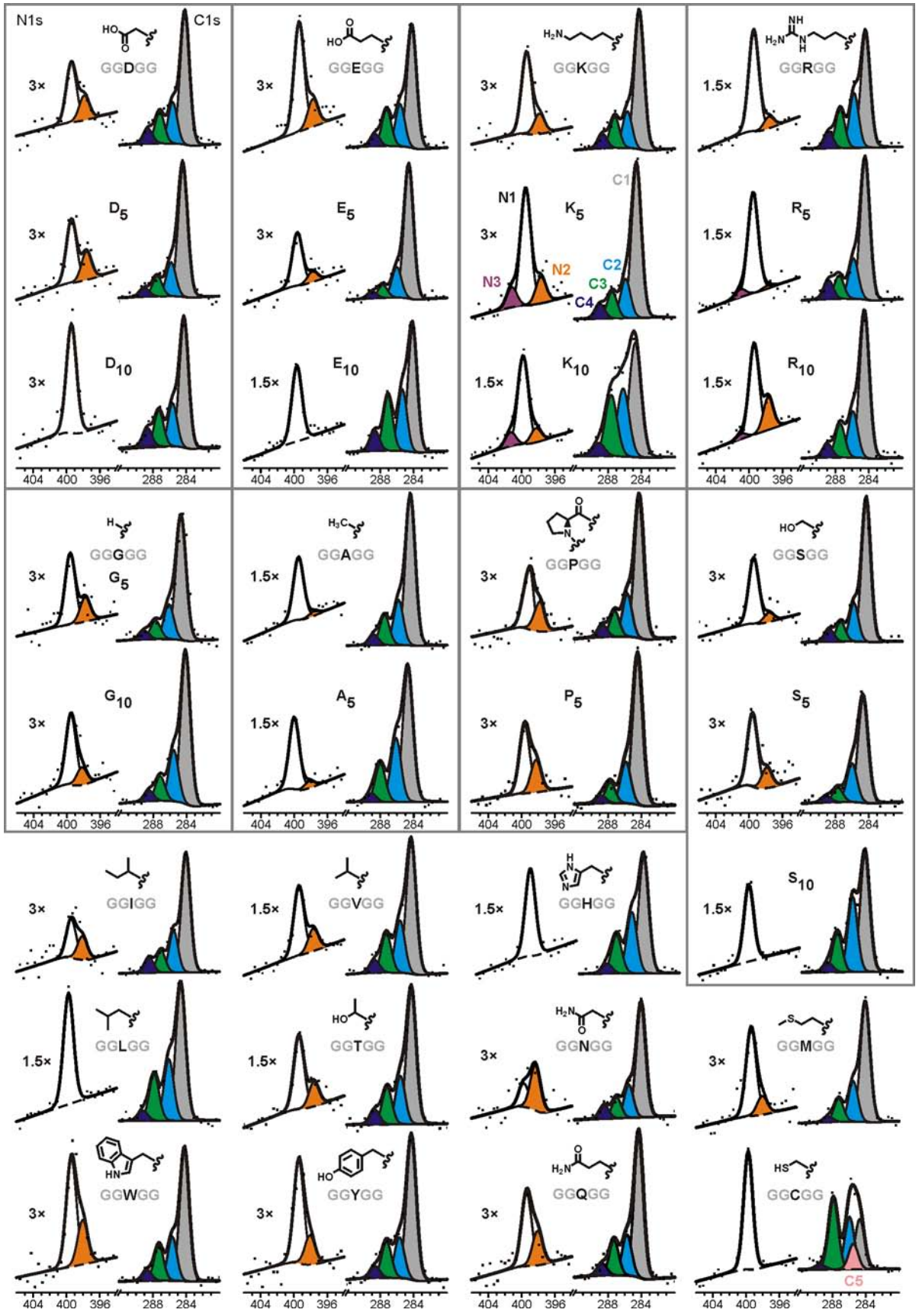

Figure 3. Representative N 1s and C 1s spectra for GG−X−GG, X_5, and X_{10} peptides. Structures of "X" residues are shown as insets; fit components are shaded; N 1s intensity is scaled up where indicated.

dx.doi.org/10.1021/ja404346p | J. Am. Chem. Soc. 2013, 135, 15040−15052

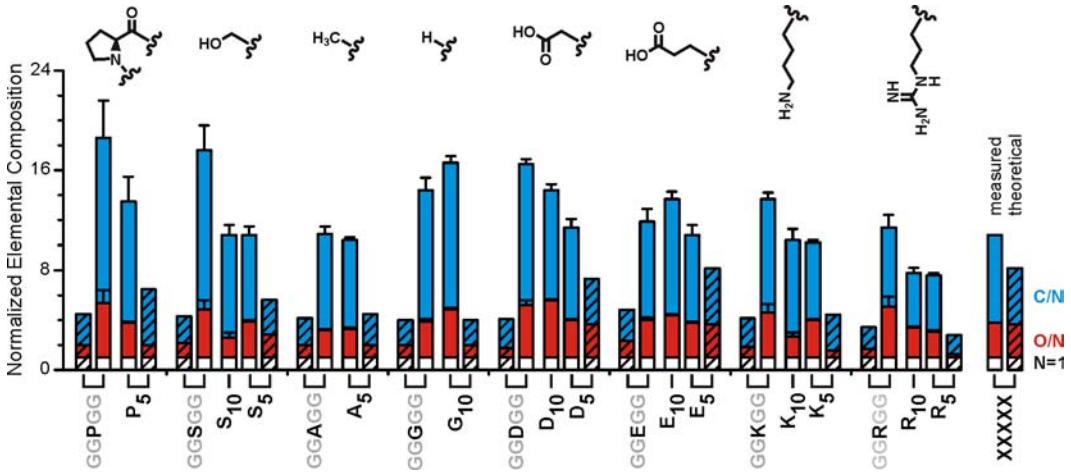

Figure 4. Elemental composition of peptide films adsorbed on gold. The data are shown for GG−X−GG, X_5, and X_{10} (where available) peptides of the "X" residues (shown as insets) that produced water-soluble homo-oligopeptides. Only the upper limits of the symmetric 95% C.I. ($n \geq 3$) are shown for clarity. As indicated in the legend, elemental ratios expected from the theoretical stoichiometry are shown by hatched columns adjacent to the corresponding measured values for GG−X−GG and X_5. The three portions of each column indicate the relative amount of nitrogen (white, set to unity in each case), oxygen (red, O/N ratio), and carbon (blue, C/N ratio); the graphical notation is explained in the Supporting Information (Figure S1).

acids, with GGFGG being the lone exception. Because we detected no nitrogen-containing species on the blank-buffer controls (Figure 2, bottom), we estimated the relative surface densities of the peptides by normalizing the N/Au atomic % ratio by the average number of nitrogen atoms per residue in the peptide, in an approach similar to that used for quantification of DNA surface densities on gold.[29−31]

Figure 6 shows the relative surface densities of GG−X−GG peptides adsorbed on gold and highlights several important aspects of their adsorption. First, we observed a significant variability in the measured surface densities. To determine if our peptides were adsorbing in excess of a monolayer, we compared the S/Au ratio of GGCGG (0.043 ± 0.008), which adsorbs on gold specifically via its thiol group (Figure 2), to a value of 0.045 consistently reported for well-ordered self-assembled monolayers (SAM) of small alkanethiols on gold.[56,58] Ulman et al. reported that alkanethiol molecules occupy a surface area of 21.4 Å^2 on gold.[57] In comparison, using a simple approximation for the spherical volume (V) of a protein based on its molecular weight (MW)[59]

$$V = \frac{\pi d^3}{6} = (1.21 \times \mathrm{MW})\text{Å}^3/\mathrm{molecule} \quad (2)$$

and estimating the area blocked by one peptide on the surface as its diameter (d) squared, we estimate the footprint of GGCGG as ca. 87 Å^2. The high S/Au ratio observed for GGCGG thus suggests that it is forming a packed monolayer of molecules that adopt conformations that maximize their packing density. Another indication of the high packing density of GGCGG is the lowest amount of carbonaceous contamination on GGCGG compared to all our samples (Figures 2−5), which is consistent with observations for other densely packed biomolecular films.[29,31] We note that the GG−X−GG peptides are broadly divided into those producing medium surface density (ca. 1/2 that of GGCGG) and those producing low surface density (ca. 1/4 that of GGCGG). Given that the range of estimated footprints (eq 2) of the GG−X−GG peptides is only 79−95 Å^2, the vast differences that we observe in the relative surface densities of the peptides cannot be solely attributed to size variations, but may reflect more relaxed surface-bound conformations of the peptides that produce low surface densities.

The variability of surface densities in Figure 6 confirms that the adsorption of the GG−X−GG peptides on gold is dominated by the central "guest" X residues, rather than by the flanking Gly residues or other common features, such as the peptide backbone or terminal groups. This assessment is further supported by noting that G_5 peptide produced one of the lowest surface densities, indicating that Gly residues have low intrinsic affinity for gold. In contrast to similarly short DNA strands that readily adsorb on gold surfaces,[30,32−34,60] the low surface densities of these model peptides are consistent with the hypothesis that cooperative binding plays a significant role in the surface adsorption of peptides and proteins.

Because we measured the concentrations of our stock peptide solutions based on the nominal weight of lyophilized powder, we sought to ensure that any uncertainties in the actual molecular concentrations were not predominantly responsible for differences in surface densities reported in Figure 6. To test the effect of peptide solution concentration on the surface adsorption, we adsorbed several peptides from incubation solutions of different concentrations (Figure 7). The polar and nonpolar central residues exhibited a significant variability in surface densities (Figure 6); therefore, three peptides were chosen from each of those groups to represent high, medium, and low surface density ranges. The density variation was small for charged peptides in Figure 6, so only GGKGG was tested for effects of the solution concentration. We note that the upper limit of uncertainty for determining peptide concentrations in aqueous solutions has been estimated elsewhere as ca. 20% for most GG−X−GG sequences.[40] Accordingly, Figure 7 verifies that even for peptides that do show a strong dependence of surface adsorption on solution concentration, the surface densities produced from 0.8 mM (hatched columns) and 1.0 mM (saturated solid shading) solutions are not statistically different. The data in Figure 7 also indicate that for polar and charged peptides even a 10-fold change in concentration did not make a difference; thus, we conclude that

dx.doi.org/10.1021/ja404346p | J. Am. Chem. Soc. 2013, 135, 15040−15052

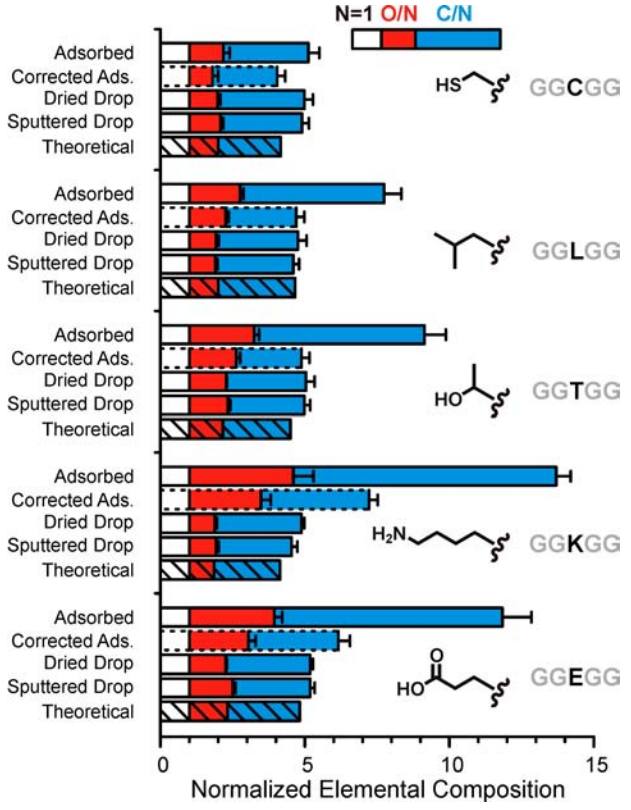

Figure 5. Evaluation of sample purity for model peptides adsorbed on gold. Normalized C/N and O/N elemental ratios are shown for five representative peptides. A set of bars for each GG−X−GG peptide (sequence and "X" residue indicated on the right) includes the measured ("adsorbed") and corrected (dashed outline, "corrected ads.") data for adsorbed peptide films as well as reference ratios for drops of the stock peptide solution ("dried" for as-deposited dried drops, "sputtered" for each drop after light sputter cleaning by low-energy Ar^+ ions) and "theoretical" stoichiometries (hatched). The three portions of each bar indicate the relative amount of nitrogen (white, set to unity in each case), oxygen (red, O/N ratio), and carbon (blue, C/N ratio). Only the upper limits of 95% C.I. ($n \geq 3$) are shown for clarity.

our relative surface densities are not significantly affected by any uncertainty in the concentration of peptides in solution.

Figure 8 indicates the relative surface densities of the adsorbed model peptides by the areas of the colored squares, which are proportional to the number of peptide *residues* per area (N/Au ratios are tabulated in the Supporting Information, Table S2). We chose normalization based on the surface density of residues rather than molecules to provide a direct comparison of the relative adsorption of peptides that have different chain lengths. The relative surface densities of the GG−X−GG peptides are represented by the orange squares, which are labeled by the corresponding "X" residues. For residues that are also represented in the X_5 and X_{10} homo-oligopeptides series—that is, those for which the X_5 and X_{10} variants were sufficiently soluble to perform adsorption experiments—the relative densities are indicated, respectively, by the green and purple squares (GG−X−GG and X_5 sequences are the same for X═G, as reflected by the combination of orange and green colors in the G square). Thin partial outlines around the corners of each square indicate the upper limits of 95% C.I. ($n \geq 3$), as explained in the Supporting Information (Figure S1).

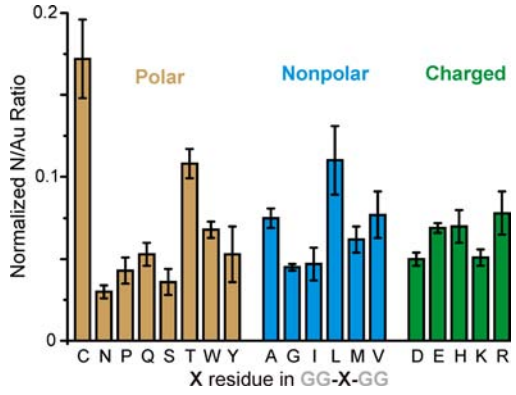

Figure 6. Relative surface densities of GG−X−GG peptides adsorbed on gold. Normalized N/Au XPS ratios are used to estimate the molecular surface densities of adsorbed peptides. The "X" central residues of GG−X−GG sequences are indicated along the bottom axis and used to group and color-code the data. To reach the maximum quasi-equilibrium surface densities of GG−X−GG peptides, clean gold substrates were incubated in 1 mM peptide solutions in 10 mM sodium phosphate (pH = 7.0) for 24 h. Error bars indicate 95% C.I. ($n \geq 3$).

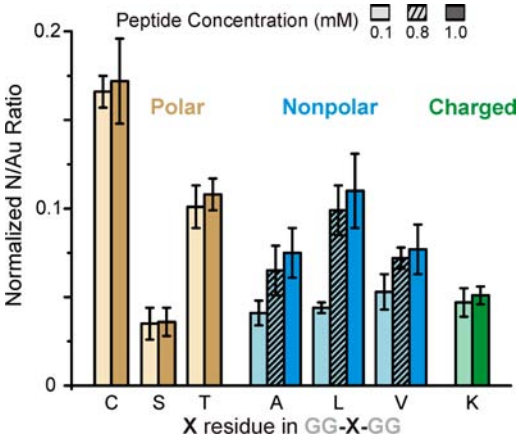

Figure 7. Effects of the peptide solution concentration on the adsorption of GG−X−GG peptides on gold. Peptide sequences are indicated along the bottom axis; the data are grouped and color-coded based on the electrostatic properties of the "X" residues. To reach the maximum quasi-equilibrium surface densities of model peptides, gold substrates were incubated in peptide solutions of the indicated concentrations (light shading = 0.1 mM, hatched = 0.8 mM, saturated shading = 1.0 mM) in 10 mM sodium phosphate (pH = 7.0) for 24 h. The intermediate peptide concentration of 0.8 mM (hatched columns) was only tested for the nonpolar GG−X−GG peptides because they exhibited significantly different surface densities when adsorbed from the 0.1 and 1.0 mM solutions. Error bars indicate 95% C.I. ($n \geq 3$).

The diagram in Figure 8 is organized into several overlapping areas (indicated by colored lines and text labels) that correspond to the physical and chemical properties of the peptide residues, following a general classification of the 20 proteinogenic amino acids suggested by Sarikaya et al.[61] We have arranged the layout of the diagram to place peptides containing structurally similar residues near one another (chemical structures of the residues are shown as insets).

Overview of Peptide Adsorption on Gold. The absence of a clear overall pattern in the variation of the measured surface densities across the physicochemical-property groupings (colored outlines in Figure 8) clearly indicates that no single

dx.doi.org/10.1021/ja404346p | J. Am. Chem. Soc. 2013, 135, 15040−15052

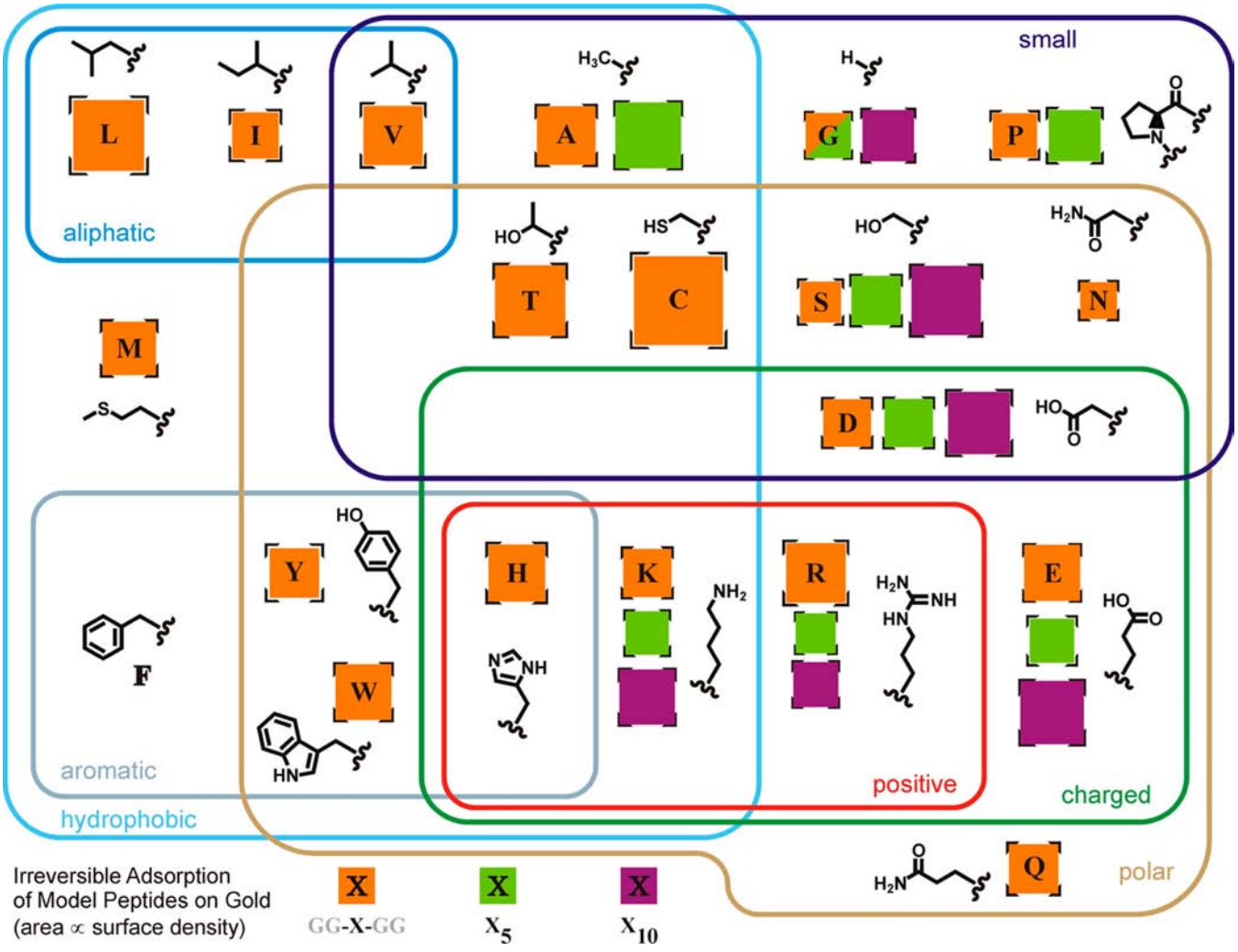

Figure 8. Relative surface densities of model peptides adsorbed on gold. Normalized N/Au XPS ratios are used to estimate the molecular surface densities of adsorbed peptides (residues/area), which are indicated by the areas of the squares. The "X" residues for each group of peptides are indicated by bold capital letters; the model sequences are indicated by the colors: orange for GG−X−GG, green for X_5, and purple for X_{10}. Colored lines and text indicate the classification of peptides by the properties of the "X" residues, which has been adapted from Sarikaya et al.[61] To reach the maximum quasi-equilibrium surface densities of model peptides, clean gold substrates were incubated in aqueous (10 mM sodium phosphate, pH = 7.0) peptide solutions (1 mM for GG−X−GG and X_5, 0.5 mM for X_{10}) for 24 h. Partial outlines around corners of each square indicate upper limits of 95% C.I. ($n \geq 3$); the graphical notation is explained in the Supporting Information (Figure S1).

parameter dominates the adsorption of our model peptides, even in the context of a relatively simple model system. This finding is perhaps not unexpected, given the diversity of the intrinsic properties and their combinations across the entire set of peptides (e.g., as reflected in complex overlapping patterns of the colored outlines in Figure 8).

Gold is an excellent conductor: therefore, electrostatic forces, including those described by the classical image-charge and induced-polarization models, can be expected to play a role in peptide adsorption. We observe that GG−X−GG peptides of all the charged central residues consistently adsorb at comparable surface densities, roughly half that of GGCGG (Figure 6). In contrast, GG−X−GG peptides of polar central residues show more variability in their adsorption, presumably because the polar side chains interact with both the gold surface and the solvent in a more complex manner than do the charged residues. When we compared pairs of peptides containing similar charged and polar residues (E vs Q, D vs N), we observed a trend for higher surface densities for peptides containing charged vs polar residues. We can rule out, however, an initial charge of the surface (or near-surface solution layer) as the dominant factor, because in that case dramatic differences would be expected in the adsorption of positive vs negative peptides, whereas we find that comparable surface densities are produced by both positive and negative GG−X−GG peptides of K, R, D, and E residues.

Peptides with Nonpolar Residues. The adsorption of GG−X−GG peptides of nonpolar central residues is the most variable of the three groups in Figure 6 and includes the most intriguing pair of results. Leu and Ile are structural isomers that have identical chemical compositions, yet GGLGG adsorbs on gold almost as readily as does GGCGG, while GGIGG adsorbs at a much lower level. The CD data in Figure 1 indicate that neither peptide is structured in aqueous solution, which largely rules out conformation restrictions as an explanation of the difference in their adsorption behavior.

We considered the XPS data in more detail to help us identify some possible reasons for the discrepancy between GGLGG and GGIGG. As we noted already, multiple spectra in Figure 3 include a small N2 component (shaded in orange)

dx.doi.org/10.1021/ja404346p | J. Am. Chem. Soc. 2013, 135, 15040−15052

shifted to lower BE = 397.7−398.3 eV, which is consistent with amide/amine groups that are interacting with inorganic substrates via contacts that involve significant charge transfer.[29,31,62] The N 1s spectrum of GGCGG does not contain this N2 component, presumably because the high affinity for gold of the thiol group in GGCGG causes displacement of any weakly bound amide groups. Notably, the N2 component is also missing in the spectrum of GGLGG, suggesting that it adopts an adsorbed conformation similar to that of GGCGG, i.e., adsorbs via its central Leu residue—perhaps as a means of minimizing the exposure of hydrophobic Leu side chain to aqueous solvent—and not via other common peptide−surface interactions.

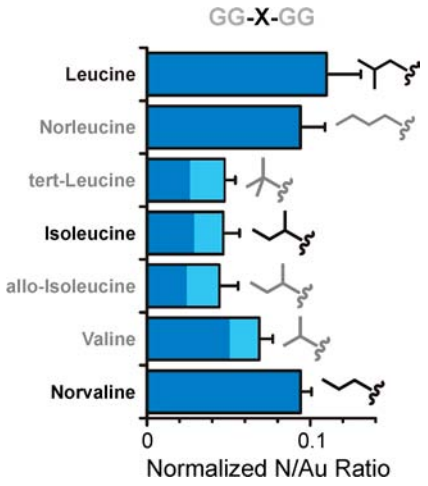

Figure 9. Normalized N/Au XPS intensity ratios of GG−X−GG peptides of Leu and Val structural isomers. Chemical structures of the central "X" residues are shown on the right. The bars are shaded to correspond to the percentage of the N 1s peak comprising the components at BE = 399.4−399.9 eV (dark shading) or BE = 397.7−398.3 eV (light shading).

To explore further the mechanisms that are responsible for the difference in surface densities of GGLGG and GGIGG, we investigated the adsorption behavior of GG−X−GG peptides where X was one of the Leu structural isomers, norleucine (Nle), *allo*-Ile, and *tert*-leucince (Tle), or the Val structural isomer, norvaline (Nva). CD revealed that all of the isomers are weakly structured in aqueous buffer (see Supporting Information, Figure S2) without any substantial differences in solution conformation that might explain the differences in their relative surface densities (Figure 9). We observed no statistical difference between the surface coverage of GGLGG and the two isomers having unbranched side chains, Nle and Nva, whereas Val, Ile, *allo*−Ile, and Tle residues—all of which have β-branched side chains, that is, side chains in which the β carbon (the first carbon in the side chain) is branched—adsorbed at significantly lower levels. Upon inspection of the N 1s spectra (data not shown), we note that the spectra for Leu, Nle, and Nva are similar in that they contain a single N1 component at BE = 399.7 ± 0.3 eV, which suggests that the side chains of the host Gly residues are not interacting with the gold surface. In contrast, the N 1s spectra of the isomers adsorbing at lower densities, Val, Ile, *allo*−Ile, and Tle, all exhibit a second N2 component at BE = 398.0 ± 0.3 eV indicating that a portion of the peptide backbone is interacting with the gold surface via contacts that involve significant charge transfer.[29,31] These data suggest that the difference we observe in the adsorption behavior of GGLGG and GGIGG arises from the location of the branched carbon (γ−C for Leu, β−C for Ile) influencing the orientation in which the peptide adsorbs to the gold surfaces. This effect may arise from steric crowding between the β-carbon substituents and the carbonyl group in the backbone.

Hydrophilic vs Hydrophobic Side Chains. Rearrangement of hydrophobic and hydrophilic components in water is an important factor that determines the structure and function of natural proteins. Examining the areas of orange squares in Figure 8 reveals that overall the GG−X−GG peptides containing hydrophobic central residues produced higher surface densities on gold than did peptides containing hydrophilic central residues. We rationalize this general trend by considering that the interaction of hydrophobic side chains is likely more energetically favorable with the gold surface than with the aqueous solvent. However, when comparing GG−X−GG peptides composed of residues with similar structures, we observe that hydrophobicity is not the dominating factor in surface adsorption—as small side chain changes that increase hydrophobicity can produce increased (T vs S, A vs G, L vs V, Q vs N, E vs D) or unchanged (V vs A, K vs Q) surface densities on gold (Figures 6 and 8).

Hydrophobic and hydrophilic side chains also produce different trends in surface density as a function of the side chain size (Figure 8). The GG−X−GG peptides containing guest residues having small hydrophobic side chains (A, T, V) produce larger surface densities than do peptides with larger hydrophobic side chains (K, H, W, Y). For GG−X−GG peptides containing charged and polar guest residues, the surface densities corresponding to smaller side chains (S, N, D) are lower than those corresponding to larger side chains (H, K, R, E, Q). The difference in the effect of the size of the side chains further suggests that hydrophobic and hydrophilic side chains adsorb to gold via different mechanisms.

The higher surface densities produced by GG−X−GG peptides containing hydrophobic guest residues may be in part related to the shift in equilibrium between peptides in solution and on the surface, as indicated by the solution concentration dependence of their surface adsorption (Figure 7). For polar and charged peptides, we observed no significant difference between adsorption from 0.1 mM vs 1 mM solutions. In contrast, the adsorption is significantly increased from the most concentrated solutions of the peptides with nonpolar central residues.

Length and Composition: GG−X−GG, X_5, X_{10}. The penta and deca (green and purple squares in Figure 8) variants of homo-oligopeptides generally follow the same trend as the GG−X−GG versions of the same central residues (Figure 6). However, in contrast to the GG−X−GG peptides, for which both positive and negative charges produce similar surface densities, no clear trends emerge for homo-oligopeptides as a function of their charge. For K, R, and E, the surface density drops from GG−X−GG to X_5 and then increases from X_5 to X_{10}; only for K, D, and E does the increased density for X_{10} surpass the GG−X−GG value. The drop in surface density from GG−X−GG to X_5 may be associated with increased peptide−peptide repulsion, i.e., related to the charge but not necessarily the surface affinity of the residues. The magnitude of the increase from X_5 to X_{10}, in turn, is likely determined by a competition between the increased cooperativity (as discussed below) and electrostatic repulsion. We conclude that, like

dx.doi.org/10.1021/ja404346p | J. Am. Chem. Soc. 2013, 135, 15040−15052

hydrophobicity, charge appears to be a contributing but not a dominant factor in determining the adsorption of peptides on gold.

Doubling the length from pentamers to decamers increases the surface density produced by all the homo-oligopeptides (purple squares are larger than green ones in Figure 8). This observation is consistent with the general expectation for oligomers of monomers that do not have a high affinity for the surface: the increased length likely enables cooperativity, i.e., increases the probability that, while not all of the weakly interacting residues become attached to the surface irreversibly, enough of them are in contact with the surface at any given time to keep the oligomer from leaving the surface. The generally small increase of surface densities from pentamers to decamers suggests that for our model oligopeptides at least one in five residues remains bound to gold at all times, limiting the cooperative gains from increasing the length from five to ten residues. The largest change of surface density with length is observed for Ser homo-oligopeptides; however, as previously discussed, the behavior of Ser homo-oligopeptides is most likely associated with the changes in their secondary structure between S_5 and S_{10} oligomers (Figure 1). For example, S_{10} may form large β-sheet aggregates in solution,[49,50] which subsequently absorb to the surface. Alternatively, a few S_{10} chains arranged in an antiparallel β sheet and adsorbed on the surface could serve as a template for further adsorption of S_{10} from solution.

Solvent Effects. A comprehensive survey of how surface adsorption of model peptides changes across a broad range of solvents falls beyond the scope of this work. Accordingly, we only tested trifluoroethanol (TFE), as a solvent less polar than water but still capable of dissolving our peptides. Figure 10 shows our investigation of three potential solvent effects on surface adsorption: peptide solubility, peptide secondary structure, and surface contamination.

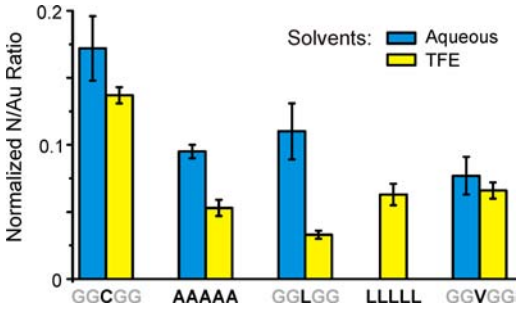

Figure 10. Solvent effects on the adsorption of pentapeptides on gold. Four model peptides (sequences indicated along the bottom axis) were deposited from 1 mM solutions in an aqueous (10 mM sodium phosphate, pH = 7.0) buffer (blue) and in TFE (yellow). The hydrophobic L_5 peptide is not soluble in water, but was added to the TFE series as a control. Error bars indicate 95% C.I. ($n \geq 3$).

For GGCGG, which adsorbs via specific thiol–gold interactions, we noted only a small decrease in the surface density achieved from TFE vs aqueous buffer. In contrast, the surface density of GGLGG and A_5 plummeted when adsorbed from TFE, a difference that we attribute to the greater solubility of the hydrophobic peptides in TFE vs aqueous buffer. This inference is further supported by a minimal change in adsorption from TFE vs aqueous buffer for the relatively less hydrophobic GGVGG. The data in Figure 10 thus suggest that preferential partitioning from the solvent toward the surface may play a role in increasing the surface densities of the most hydrophobic sequences deposited from aqueous buffer (Figure 8). The significant adsorption of the hydrophobic sequences in Figure 10 from TFE, however, does indicate that hydrophobic residues do have affinities for gold. The increase of surface density from GGLGG to L_5 when deposited in TFE suggests that cooperative interactions between Leu and gold may be enhancing the adsorption of L_5 (L_5 also exhibits secondary structure in TFE, as indicated by the CD data in the Supporting Information, Figure S3).

The final purpose of the experiments in Figure 10 was to test for any effects of competitive coadsorption of peptides and aliphatic-carbon contaminants (the latter are more soluble in TFE than in water). All four test peptides in Figure 10 adsorbed in smaller amounts from TFE than from aqueous buffer, suggesting that any aliphatic-carbon contaminants that may be present in the incubation solutions do not have a significant effect on the surface adsorption of our model peptides.

■ CONCLUSIONS

We selected a series of model peptides for systematically evaluating the interactions between peptide residues and surfaces in aqueous solutions. The series includes GG–X–GG "host-guest" peptides, in which the guest X residues correspond to 19 out of 20 proteinogenic amino acids, as well as additional water-soluble homo-oligopeptides (penta- and decamers). Solution CD measurements confirmed that GG–X–GG peptides lack significant secondary structure, thus avoiding possible interference in surface adsorption from the structure of peptides.

Gold substrates with peptides irreversibly adsorbed from aqueous buffer were quantitatively analyzed by XPS, revealing a broad range of the maximum quasi-equilibrium surface densities, corroborating our hypothesis that interactions of these peptides with gold are dominated by their central residues. The highest surface densities under all conditions in our work have been produced by GGCGG, which attaches to gold via specific thiol–gold interaction. For the other GG–X–GG peptides, the highest surface densities are produced by sequences with hydrophobic central residues, followed by those with charged central residues, and those with polar ones. Interestingly, we do not observe a significant difference between adsorption of GG–X–GG peptides with central residues having charges of opposite signs. Considering the details of the observed trends, we conclude that neither the electrostatic nor hydrophobic interactions generally dominate the adsorption of GG–X–GG peptides: for charged and polar central residues, the surface densities correlate with the size of the side chains rather than the electrostatic properties, while for hydrophobic residues, side chain changes that increase hydrophobicity can produce an increased or unchanged surface density. The surface densities of the most hydrophobic model peptides decrease when they are adsorbed from TFE rather than from aqueous buffer, highlighting that peptide–solvent interactions also play a role in the adsorption behavior of the peptides. The low overall surface activities of these model peptides (none produced surface densities comparable to that of GGCGG) reinforce the hypothesis that cooperative binding is important for surface attachment of proteins, which readily adsorb on most artificial surfaces.

Finally, we observe an intriguing discrepancy between the adsorption of GGLGG and GGIGG peptides. The physical and

chemical properties of these peptides are almost identical, as their central Leu and Ile residues are structural isomers, yet the two peptides exhibit a dramatic difference in their adsorption on gold. Upon examination of the adsorption behavior of other isomers of Leu, as well as Val, we discovered a correlation between the adsorption behavior of the isomers and branching in the side chain. The β-branched isomers (Ile, *allo*−Ile, Tle, and Val) adsorbed at significantly lower surface densities than their γ-branched (Leu) or unbranched (Nle and Nva) counterparts. Furthermore, the N 1s spectra suggest that steric effects from the branched β carbon drive interactions between the peptide backbone and the gold surface, whereas there was no evidence of such interactions with GG−X−GG peptides of Leu, Nle, and Nva.

■ ASSOCIATED CONTENT

Supporting Information

Elemental ratios and normalized N/Au ratios for all the GG−X−GG, X_5, and X_{10} peptides. CD spectra of model peptides in 10 mM sodium phosphate and TFE. This material is available free of charge via the Internet at http://pubs.acs.org.

■ AUTHOR INFORMATION

Corresponding Authors

*E-mail: thomas.clark@nrl.navy.mil.
*E-mail: dmitri.petrovykh@inl.int.

Present Address

D. Y. P., International Iberian Nanotechnology Laboratory (INL), Avenida Mestre José Veiga, 4715−330 Braga, Portugal.

Notes

The authors declare no competing financial interest.

■ ACKNOWLEDGMENTS

This work was supported by the Office of Naval Research (ONR) and the Air Force Office of Scientific Research (AFOSR). K.P.F. thanks the National Research Council for a Postdoctoral Fellowship at NRL during the initial stages of this project. D.Y.P. and T.D.C. thank Dr. Lloyd Whitman for his help in initiating this project.

■ REFERENCES

(1) Addadi, L.; Weiner, S. *Proc. Natl. Acad. Sci. U. S. A.* **1985**, *82*, 4110−4114.
(2) Njegic-Dzakula, B.; Brecevic, L.; Falini, G.; Kralj, D. *Cryst. Growth Des.* **2009**, *9*, 2425−2434.
(3) Nonoyama, T.; Kinoshita, T.; Higuchi, M.; Nagata, K.; Tanaka, M.; Sato, K.; Kato, K. *Langmuir* **2011**, *27*, 7077−7083.
(4) Gower, L. B.; Odom, D. J. *J. Cryst. Growth* **2000**, *210*, 719−734.
(5) Sarikaya, M.; Tamerler, C.; Jen, A. K. Y.; Schulten, K.; Baneyx, F. *Nat. Mater.* **2003**, *2*, 577−585.
(6) Sander, M.; Pignatello, J. J. *Environ. Sci. Technol.* **2005**, *39*, 1606−1615.
(7) Adhikari, B.; Banerjee, A. *Soft Matter* **2011**, *7*, 9259−9266.
(8) So, C. R.; Hayamizu, Y.; Yazici, H.; Gresswell, C.; Khatayevich, D.; Tamerler, C.; Sarikaya, M. *ACS Nano* **2012**, *6*, 1648−1656.
(9) Zorbas, V.; Smith, A. L.; Xie, H.; Ortiz-Acevedo, A.; Dalton, A. B.; Dieckmann, G. R.; Draper, R. K.; Baughman, R. H.; Musselman, I. H. *J. Am. Chem. Soc.* **2005**, *127*, 12323−12328.
(10) Feyer, V.; Plekan, O.; Ptasinska, S.; Iakhnenko, M.; Tsud, N.; Prince, K. C. *J. Phys. Chem. C* **2012**, *116*, 22960−22966.
(11) Vallee, A.; Humblot, V.; Pradier, C.-M. *Acc. Chem. Res.* **2010**, *43*, 1297−1306.
(12) Holinga, G. J.; York, R. L.; Onorato, R. M.; Thompson, C. M.; Webb, N. E.; Yoon, A. P.; Somorjai, G. A. *J. Am. Chem. Soc.* **2011**, *133*, 6243−6253.
(13) Willett, R. L.; Baldwin, K. W.; West, K. W.; Pfeiffer, L. N. *Proc. Natl. Acad. Sci. U. S. A.* **2005**, *102*, 7817−7822.
(14) Mermut, O.; Phillips, D. C.; York, R. L.; McCrea, K. R.; Ward, R. S.; Somorjai, G. A. *J. Am. Chem. Soc.* **2006**, *128*, 3598−3607.
(15) Horinek, D.; Serr, A.; Geisler, M.; Pirzer, T.; Slotta, U.; Lud, S. Q.; Garrido, J. A.; Scheibel, T.; Hugel, T.; Netz, R. R. *Proc. Natl. Acad. Sci. U.S.A.* **2008**, *105*, 2842−2847.
(16) Apte, J. S.; Collier, G.; Latour, R. A.; Gamble, L. J.; Castner, D. G. *Langmuir* **2010**, *26*, 3423−3432.
(17) Slocik, J. M.; Naik, R. R. *Chem. Soc. Rev.* **2010**, *39*, 3454−3463.
(18) Weidner, T.; Apte, J. S.; Gamble, L. J.; Castner, D. G. *Langmuir* **2010**, *26*, 3433−3440.
(19) Avouris, P.; Persson, B. N. J. *J. Phys. Chem.* **1984**, *88*, 837−848.
(20) Persson, B. N. J.; Andersson, S. *Phys. Rev. B* **1984**, *29*, 4382−4394.
(21) Raut, V. P.; Agashe, M. A.; Stuart, S. J.; Latour, R. A. *Langmuir* **2005**, *21*, 1629−1639.
(22) O'Brien, C. P.; Stuart, S. J.; Bruce, D. A.; Latour, R. A. *Langmuir* **2008**, *24*, 14115−14124.
(23) Vellore, N. A.; Yancey, J. A.; Collier, G.; Latour, R. A. *Langmuir* **2010**, *26*, 7396−7404.
(24) Wei, Y.; Latour, R. A. *Langmuir* **2008**, *24*, 6721−6729.
(25) Storhoff, J. J.; Elghanian, R.; Mirkin, C. A.; Letsinger, R. L. *Langmuir* **2002**, *18*, 6666−6670.
(26) Shi, Z.; Chen, K.; Liu, Z.; Ng, A.; Bracken, W. C.; Kallenbach, N. R. *Proc. Natl. Acad. Sci. U. S. A.* **2005**, *102*, 17964−17968.
(27) Schwarzinger, S.; Kroon, G. J. A.; Foss, T. R.; Chung, J.; Wright, P. E.; Dyson, H. J. *J. Am. Chem. Soc.* **2001**, *123*, 2970−2978.
(28) He, L.; Navarro, A. E.; Shi, Z.; Kallenbach, N. R. *J. Am. Chem. Soc.* **2012**, *134*, 1571−1576.
(29) Petrovykh, D. Y.; Kimura-Suda, H.; Whitman, L. J.; Tarlov, M. J. *J. Am. Chem. Soc.* **2003**, *125*, 5219−5226.
(30) Kimura-Suda, H.; Petrovykh, D. Y.; Tarlov, M. J.; Whitman, L. J. *J. Am. Chem. Soc.* **2003**, *125*, 9014−9015.
(31) Petrovykh, D. Y.; Kimura-Suda, H.; Tarlov, M. J.; Whitman, L. J. *Langmuir* **2004**, *20*, 429−440.
(32) Opdahl, A.; Petrovykh, D. Y.; Kimura-Suda, H.; Tarlov, M. J.; Whitman, L. J. *Proc. Natl. Acad. Sci. U. S. A.* **2007**, *104*, 9−14.
(33) Schreiner, S. M.; Shudy, D. F.; Hatch, A. L.; Opdahl, A.; Whitman, L. J.; Petrovykh, D. Y. *Anal. Chem.* **2010**, *82*, 2803−2810.
(34) Schreiner, S. M.; Hatch, A. L.; Shudy, D. F.; Howard, D. R.; Howell, C.; Zhao, J.; Koelsch, P.; Zharnikov, M.; Petrovykh, D. Y.; Opdahl, A. *Anal. Chem.* **2011**, *83*, 4288−4295.
(35) Yoshinari, M.; Kato, T.; Matsuzaka, K.; Hayakawa, T.; Shiba, K. *Biofouling* **2010**, *26*, 103−110.
(36) Seker, U. O. S.; Wilson, B.; Sahin, D.; Tamerler, C.; Sarikaya, M. *Biomacromolecules* **2009**, *10*, 250−257.
(37) Mrksich, M.; Sigal, G. B.; Whitesides, G. M. *Langmuir* **1995**, *11*, 4383−4385.
(38) Benesch, J.; Askendal, A.; Tengvall, P. *Colloids Surf., B* **2000**, *18*, 71−81.
(39) Fears, K. P.; Creager, S. E.; Latour, R. A. *Langmuir* **2008**, *24*, 837−843.
(40) Fears, K. P.; Petrovykh, D. Y.; Clark, T. D. *Biointerphases* **2013**, *8*, 20.
(41) Seah, M. P.; Gilmore, L. S.; Beamson, G. *Surf. Interface Anal.* **1998**, *26*, 642−649.
(42) Hesse, R.; Streubel, P.; Szargan, R. *Surf. Interface Anal.* **2007**, *39*, 381−391.
(43) Scofield, J. H. *J. Electron Spectrosc. Relat. Phenom.* **1976**, *8*, 129−137.
(44) Jablonski, A.; Powell, C. J. *Surf. Sci. Rep.* **2002**, *47*, 35−91.
(45) Tanuma, S.; Powell, C. J.; Penn, D. R. *Surf. Interface Anal.* **1994**, *21*, 165−176.

(46) Sreerama, N.; Manning, M. C.; Powers, M. E.; Zhang, J. X.; Goldenberg, D. P.; Woody, R. W. *Biochemistry* **1999**, *38*, 10814−10822.
(47) Woody, A. Y. M.; Woody, R. W. *Biopolymers* **2003**, *72*, 500−513.
(48) Chakrabartty, A.; Kortemme, T.; Padmanabhan, S.; Baldwin, R. L. *Biochemistry* **1993**, *32*, 5560−5565.
(49) Quadrifoglio, F.; Urry, D. W. *J. Am. Chem. Soc.* **1968**, *90*, 2760−2765.
(50) Gupta, A.; Tandon, P.; Gupta, V. D.; Rastogi, S. *Polymer* **1997**, *38*, 2389−2397.
(51) Cho, Y.; Ivanisevic, A. *J. Phys. Chem. B* **2005**, *109*, 6225−6232.
(52) Iucci, G.; Battocchio, C.; Dettin, M.; Gambaretto, R.; Di Bello, C.; Borgatti, F.; Carravetta, V.; Monti, S.; Polzonetti, G. *Surf. Sci.* **2007**, *601*, 3843−3849.
(53) Zubavichus, Y.; Shaporenko, A.; Grunze, M.; Zharnikov, M. *J. Phys. Chem. B* **2007**, *111*, 9803−9807.
(54) Lee, C.-Y.; Gong, P.; Harbers, G. M.; Grainger, D. W.; Castner, D. G.; Gamble, L. J. *Anal. Chem.* **2006**, *78*, 3316−3325.
(55) Lock, E. H.; Petrovykh, D. Y.; Mack, P.; Carney, T.; White, R. G.; Walton, S. G.; Fernsler, R. F. *Langmuir* **2010**, *26*, 8857−8868.
(56) Petrovykh, D. Y.; Kimura-Suda, H.; Opdahl, A.; Richter, L. J.; Tarlov, M. J.; Whitman, L. J. *Langmuir* **2006**, *22*, 2578−2587.
(57) Ulman, A.; Eilers, J. E.; Tillman, N. *Langmuir* **1989**, *5*, 1147−1152.
(58) Techane, S. D.; Gamble, L. J.; Castner, D. G. *J. Phys. Chem. C* **2011**, *115*, 9432−9441.
(59) Harpaz, Y.; Gerstein, M.; Chothia, C. *Structure* **1994**, *2*, 641−649.
(60) Wolf, L. K.; Gao, Y.; Georgiadis, R. M. *Langmuir* **2004**, *20*, 3357−3361.
(61) Sarikaya, M.; Tamerler, C.; Schwartz, D. T.; Baneyx, F. O. *Annu. Rev. Mater. Res.* **2004**, *34*, 373−408.
(62) Fears, K. P.; Petrovykh, D. Y.; Photiadis, S. J.; Clark, T. D. *Langmuir* **2013**, *29*, 10095−10101.